# Computer simulations of a single-laser double-gas-jet wakefield accelerator concept

R. G. Hemker, N. M. Hafz, and M. Uesaka
*Nuclear Engineering Research Laboratory, University of Tokyo, 22-2 Shirane-Shirakata, Tokai, Naka, Ibaraki, 319-1196 Japan*
(Received 10 July 2001; published 12 April 2002)

We report in this paper on full scale 2D particle-in-cell simulations investigating laser wakefield acceleration. First we describe our findings of electron beam generation by a laser propagating through a single gas jet. Using realistic parameters which are relevant for the experimental setup in our laboratory we find that the electron beam resulting after the propagation of a 0.8 $\mu$m, 50 fs laser through a 1.5 mm gas jet has properties that would make it useful for further acceleration. Our simulations show that the electron beam is generated when the laser exits the gas jet, and the properties of the generated beam, especially its energy, depend only weakly on most properties of the gas jet. We therefore propose to use the first gas jet as a plasma cathode and then use a second gas jet placed immediately behind the first to provide additional acceleration. Our simulations of this proposed setup indicate the feasibility of this idea and also suggest ways to optimize the quality of the resulting beam.

DOI: 10.1103/PhysRevSTAB.5.041301 PACS numbers: 52.38.Kd, 52.65.Rr, 41.75.Jv, 52.65.−y

## I. INTRODUCTION

The concept of a laser wakefield accelerator (LWFA) for electrons was suggested more than twenty years ago but only in recent years has laser power reached the point to experimentally investigate this idea [1–4]. The detailed theoretical analysis of the LWFA concept is difficult as well. Because of their mutual interaction, the evolution of the laser pulse, the generated plasma wave wake, and the accelerated electrons are not easily described by analytical models. Currently the only method to get a detailed understanding of the processes in a LWFA that can aid the design of experiments as well as further theoretical investigations is the use of fully self-consistent particle-in-cell (PIC) simulations.

Questions of particular interest are (1) the mechanisms by which electrons can be trapped and then accelerated using a LWFA, and (2) the quality of the beams that can be generated. To address these questions which are relevant to the experiments in our laboratory we have used 2D PIC simulations to investigate the propagation of a laser pulse through a plasma over distances similar to the ones in our experiment. As a result of our simulations we are proposing a novel setup for LWFA that uses a single laser and two gas jets.

## II. SIMULATION SETUP

The parameters of the simulations we conducted were guided by the experimental setup in our laboratory [5–7]. In the following we will first describe the simulation setup for a single 50 fs long (FWHM), linear polarized, 12 TW laser pulse with a wavelength of 0.8 $\mu$m and a Gaussian spot size of 13 $\mu$m. In simulations we model the transverse profile of the laser as a Gaussian. In contrast the longitudinal profile rises and falls symmetrically according to the form $f(x) = 10x^3 - 15x^4 + 6x^5$ with $0 \le x/L_s \le 1$ where $L_s$ is the length of the rise and fall, respectively. $L_s$ is suitably chosen to minimize the difference between the used polynomial function and a Gaussian pulse shape. Given the above spot size the 12 TW laser pulse corresponds to a peak intensity of $I = 4.7 \times 10^{18}$ W/cm$^2$ and a normalized vector potential of $a = 1.5$. This laser pulse passes through a gas jet of about 1.5 mm diameter. In our simulations we assume that the gas of the jet is completely ionized by the leading edge of the laser pulse and we will therefore use the terms plasma or gas jet interchangeably throughout this paper. The actual ionization process is not included in the simulations.

The 2D simulations were done using the recently developed fully relativistic PIC simulation code OSIRIS [8,9]. The code is a scalable parallel code and can be used for 2D as well as 3D simulations. It contains a moving window algorithm [10] that makes it possible to conduct simulations over the distances we have in our experiments with a reasonable amount of computing resources. The simulations window, which was moving with the speed of light in the propagation direction of the laser pulse and thereby following the laser as well as any high energy electrons, had in normalized units dimensions of $905c/\omega_n$ in the $x_1$ direction and $2111c/\omega_n$ in the $x_2$ direction. $\omega_n$ here is the frequency used for normalization. For convenience we choose $\omega_n = \omega_L$, the laser frequency. This normalization means that a distance of $2\pi$ in normalized units corresponds to the length of the laser wavelength $\lambda_L = 0.8$ $\mu$m. The moving window size in SI units is therefore 115 $\mu$m $\times$ 269 $\mu$m. We will use normalized as well as SI units throughout this paper. The computational grid of the simulations was $2048 \times 768$ with four particles per cell. Note that even though the simulation box moves with $c$ all calculations are done in the laboratory frame.

The simulations with a single gas jet of 1.5 mm diameter were run for a time of $12\,600\omega_n^{-1}$ ($5.35 \times 10^{-12}$ s) corresponding to a propagation distance of $12\,600c/\omega_n$ (1600 $\mu$m). The Rayleigh length for the

  

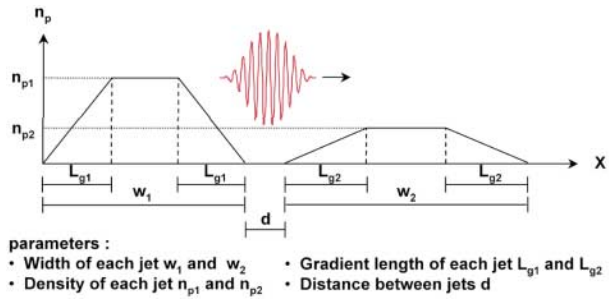


FIG. 1. (Color) A schematic of the two gas-jet concept proposed in this paper. After passing through the first gas jet the laser and the electron beam generated by it in the first gas jet will enter a second gas jet. This setup provides several controllable parameters that can be exploited in experiments.

simulated laser pulse was $X_R = 5000c/\omega_n$ (640 $\mu$m), and therefore the propagation distance was about $2.5X_R$. The time step size was $0.42\omega_n^{-1}$. For simulations with two gas jets of 1.5 mm diameter the number of time steps and therefore the propagation time and distance was doubled. The parameters described above are valid for all simulations discussed in this paper unless specific differences are mentioned.

Figure 1 shows the general setup used in our simulations to model propagation of a laser through one and two gas jets. A laser pulse is initialized in vacuum and propagates through a plasma of linearly increasing plasma density corresponding to the transition from vacuum into a gas jet. It then propagates through a region of constant density and finally passes through a region of linearly decreasing plasma density. In case of a simulation with two gas jets the laser and the high energy electrons generated in the first gas jet will then propagate through a second gas jet modeled in the same way. The figure also indicates the different parameters that, in principal, can be varied in this setup. If we assume cylindrically symmetric gas jets the length of the gradients on both sides of a given gas jet has to be, of course, the same.

As we show in the remainder of this paper the use of two gas jets makes it possible to change the parameters $w_i$, $L_{gi}$, and $n_{pi}$ of each gas jet so they are optimized for specific functions: initial beam generation for the first gas jet and additional acceleration for the second gas jet. The distance $d$ between the gas jets is an additional parameter that is available in this setup and might be useful for additional tuning.

## III. SINGLE GAS-JET RESULTS

We first discuss the results for the electron beam generation in a single gas jet. There are three distinct regions of the gas jet: the density upramp, the constant density region, and the density downramp, which should be considered separately when looking at the properties with regard to trapping background plasma electrons. We conducted first a series of simulations with density upramps of various lengths but all going up to a maximum plasma density of $7.07 \times 10^{18}$ cm$^{-3}$.

We chose this density since it was at the higher end of the range of densities that we expected to produce in experiments. At this density with a plasma wavelength of $\lambda_p = 12.4$ $\mu$m and with a laser pulse length of $L_{\mathrm{FWHM}} = 15$ $\mu$m we get a ratio of $L_{\mathrm{FWHM}}/\lambda_p = 1.21$. According to the results of a previous research [3] there is a broadened resonance maximum between the laser pulse length and the plasma wavelength around $L_{\mathrm{FWHM}}/\lambda_p = 1$ for large values of the laser strength parameter $a$. This means that there is a larger range of values (compared to the $a < 1$ regime) around $L_{\mathrm{FWHM}}/\lambda_p = 1$ where the accelerating field varies only little. We tested this with a simulation at a density of $5 \times 10^{18}$ cm$^{-3}$. The maximum accelerating field of this simulation differed by only about 10% from the maximum accelerating field of the simulations at $7.07 \times 10^{18}$ cm$^{-3}$. This indicated that with $n = 7.07 \times 10^{18}$ cm$^{-3}$ we were in this regime with a broadened maximum regime, and we therefore used this density as the maximum density in the simulations described below.

The length of the upramps varied from 500 to 0 $\mu$m (density step function). Only in the case of the step function did we find any trapping of electrons. After propagation of 500 $\mu$m in the constant density region the trapped bunch of electrons had the following properties: beam energy $\gamma = 91.4$, energy spread $\Delta E/E = 18.6\%$, normalized emittance $\epsilon_n = 70.9\pi$ mm mrad, beam length $l_{\mathrm{FWHM}} = 3.26$ $\mu$m ($10.9 \times 10^{-15}$ s), and beam charge $Q = 42.4 \times 10^{-12}$ C.

Even with a density upramp as short as 30 $\mu$m which is about twice the plasma wavelength at $7.07 \times 10^{18}$ cm$^{-3}$ we did not see any electron trapping. This indicates that the gradient length needs to be short compared to the plasma wavelength in order to see any electron trapping. Since the density gradient regions seen in experiments so far have been significantly wider [11–13] we conclude that this mechanism is unlikely to be useful in actual experiments.

No trapping of electrons occurred in any of our simulations in the region of constant density. This is consistent with the fact that the amplitude of the wakefield in the simulations was about 160 GeV/m. The cold relativistic 1D wave breaking field [14]

$$E_{\mathrm{WB}} = \sqrt{2(\gamma_p - 1)}\, E_0 \qquad (1)$$

with $E_0 = mc\omega_p/e$ and $\gamma_p = \omega_L/\omega_p$ can be used as a rough estimate for the field required for wave breaking. This value is about 9 times larger than the actual amplitude seen in the simulations.

In contrast to the density upramp and the constant density region, trapping of electrons does occur within a wide range of parameters when the laser pulse passes through the density downramp. Figure 2 shows a typical longitudinal phase space at the time when the laser pulse has just left the plasma. There are several groups of higher energy

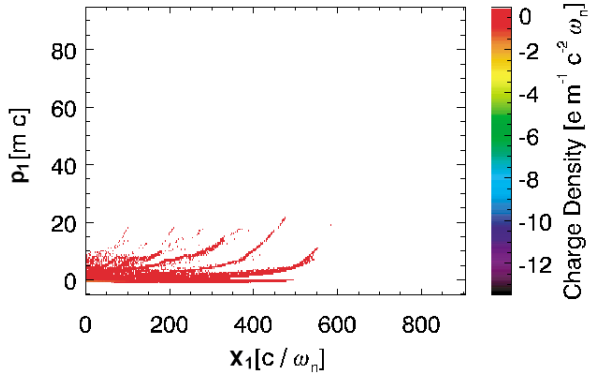


FIG. 2. (Video) A typical longitudinal phase space density plot of the plasma electrons at the time when the laser has just exited the first gas jet. The gas-jet parameters in this simulation are $w_1 = 1.5$ mm, $L_{g1} = 0.5$ mm, and $n_{p1} = 7.07 \times 10^{18}$ cm$^{-3}$. See videos 1 and 2 for the dynamic development of the phase space.

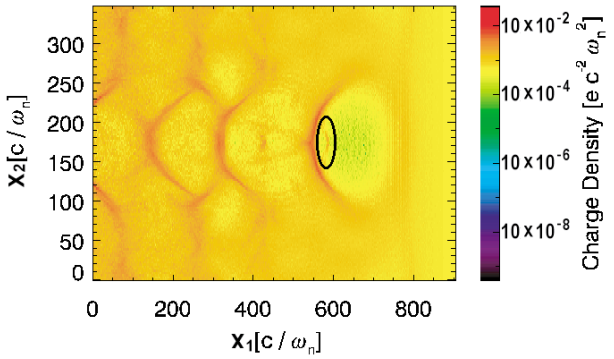


FIG. 3. (Video) The electron density in the plane of the simulation shortly before the laser leaves the plasma almost at the end of the density downramp. The laser propagates to the right. The marked group of electrons gets only at this time trapped by transverse wave breaking and then accelerated briefly until the laser and the accelerated electrons leave the plasma. The position of the marked electrons is about 120 $\mu$m away from the plasma boundary. Note that the $x_1$ axis and the $x_2$ axis of the plot use slightly different scales. See video 3 for the dynamic development of the electron density.

electrons (5–10 MeV) as well as a larger number of electrons with energies up to 5 MeV. The data shown in Fig. 2 are for a gas jet with $w_1 = 1.5$ mm, $L_{g1} = 0.5$ mm, and $n_{p1} = 7.07 \times 10^{18}$ cm$^{-3}$.

The dynamic development of the longitudinal phase space along the 500 $\mu$m density downramp is clearly seen in videos 1 and 2 accompanying this paper. Note that the first halves of these two videos are identical since they are from simulations propagating first through gas jets with identical parameters. These simulations differ in the parameters of the second gas jet used, and we will discuss those differences and their effects in the next section. With regard to trapping on the density downramp the frames that are important in these videos (and are the same in both) are from time $8568\omega_n^{-1}$ (1091 $\mu$m) to $12\,264\omega_n^{-1}$ (1561 $\mu$m).

The videos show that particle trapping occurs as soon as the laser and the wake it generates move into the density downramp. Electrons are being trapped and accelerated up to energies of about 13 MeV but then decelerated again. This deceleration is due to the fact that the plasma wavelength of the wake increases as the laser moves towards lower densities. This means that electrons that at first experience an accelerating field will soon afterwards experience a decelerating field as the plasma wavelength of the wake lengthens. The electrons that have an actual net energy gain are the ones that are being trapped and accelerated over the last 200 to 300 $\mu$m (after frame $9576\omega_n^{-1}$, corresponding to 1220 $\mu$m) before the laser completely leaves the plasma.

Our simulation results indicate that the combination of two factors allows the occurrence of wave breaking in the density downramp region. This result is consistent with previous research results by other groups [15–19]. Figure 3 and video 3 show clearly that the wave breaking that happens is transverse wave breaking, but since this wave breaking takes place only once, the laser enters the gradient region indicating that variation of the plasma wavelength along the gradient is necessary to lower the threshold for wave breaking enough for it to take place. Figure 3 shows the transverse injection of electrons into the wave. The marked group of particles is in the process of being transversely injected into the wakefield. Those particles correspond to the rightmost group of particles in Fig. 2.

The transverse injection can be seen even more clearly in video 3 that accompanies this paper. The video shows evolution of the electron density in the moving window of the simulation. While the laser enters the plasma and moves through the plasma density upramp, the plasma wavelength shortens (up to frame $4032\omega_n^{-1}$, corresponding to 513 $\mu$m). It stays constant while the laser propagates through the region of constant density (up to frame $8064\omega_n^{-1}$, corresponding to 1026 $\mu$m) and then increases again when the laser moves through the area of decreasing density (up to frame $12\,096\omega_n^{-1}$, corresponding to 1539 $\mu$m). Only during this last phase can transverse wave breaking and trapping of electrons be observed in the video.

In order to get a better idea of what kind of beams can be obtained by wave breaking and trapping in the density downramp region we did simulations where we varied systematically the length of the downramp while keeping all other parameters of the simulations, the length of the upramp, and constant density regions, as well as the maximum density, unchanged.

The results of this parameter scan are shown in Fig. 4. The beam energy $\gamma$, the energy spread $\Delta E/E$, the normalized emittance $\epsilon_n$, the beam length $l_{\mathrm{FWHM}}$, and the beam charge $Q$ are shown as functions of the density downramp gradient length $L_g$. Since we were interested in high energy electrons we included only electrons with a

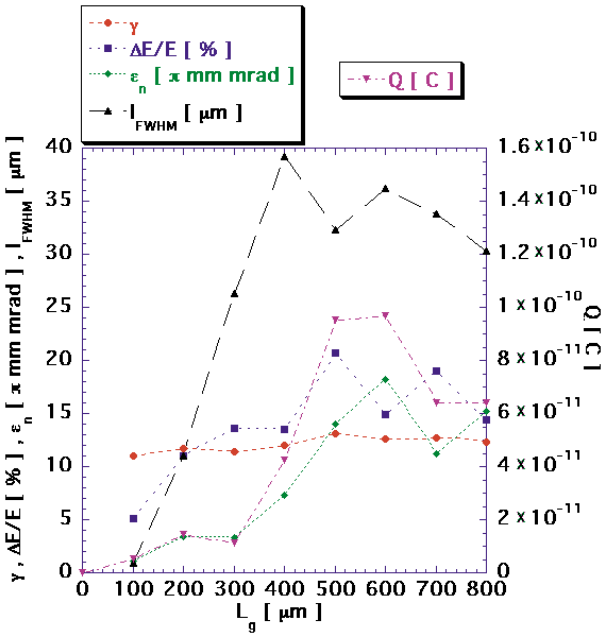


FIG. 4. (Color) Important beam characteristics as a function of the length of the density gradient on the side of the first gas jet where the laser exits it. The beam energy $\gamma$, the energy spread $\Delta E/E$, the normalized emittance $\epsilon_n$, the beam length $l_{\mathrm{FWHM}}$, and the beam charge $Q$ are shown. Only electrons with $p_1 \geq 10$ mc were included in the calculation of the numbers shown in the figure.

longitudinal momentum above 10 mc, corresponding roughly to 5 MeV energy, in the calculation of the beam quantities. The normalized emittance of the beam given here is the normalized rms emittance [20] calculated using the simulation particles. In order to calculate the total charge of the beam we make the assumption that the width of the beam in $x_3$ is the same as the rms width of the beam in $x_2$.

The first thing that should be noted is that the beam charge increases sharply with the increase in $L_g$, from no charge at $L_g = 0$ to a maximum of about 100 pC, between 500 and 600 $\mu$m. It then decreases again but more slowly. The energy, the energy spread, the emittance, and the length of the beam are all roughly following the same type of behavior. This trend is the weakest in the actual beam energy $\gamma$ since it varies only between 11 and 13 $\mathrm{mc}^2$. The trends seen in the figure are roughly consistent with the expectation that for very long density gradients the injection should disappear. Since longer simulations would have required more computational resources we were not able to test this directly beyond the data points shown in Fig. 4. The most important point of this figure is that between 500 and 600 $\mu$m all of the beam properties are quite stable, which would make an experiment quite stable to shot-to-shot jitter in the gradient length. In addition this stable range also produces the largest number of high energy electrons. The beam properties at 500 $\mu$m are a beam energy $\gamma = 13$, an energy spread $\Delta E/E = 21\%$, a normalized emittance $\epsilon_n = 14\pi$ mm mrad, a beam length $l_{\mathrm{FWHM}} = 32.3$ $\mu$m ($108 \times 10^{-15}$ s), and a beam charge $Q = 95 \times 10^{-12}$ C. We note that generating a gradient length of about 500 $\mu$m should be well within the current experimental possibilities [11–13].

We can compare these simulation results with the experimental results from the photocathode rf gun in our laboratory [21]. The measured properties of the photocathode rf gun beam are an energy $\gamma = 32$, an energy spread $\Delta E/E = 3\%$, a normalized emittance $\epsilon_n = 6\pi$ mm mrad, a beam length $l_{\mathrm{FWHM}} = 72$ $\mu$m ($240 \times 10^{-15}$ s), and a beam charge $Q = 350 \times 10^{-12}$ C. We find that the photocathode rf gun beam has significantly higher energy, higher charge, lower emittance, and lower energy spread while the beam generated in the simulation is significantly shorter.

These are clear differences but the comparison does show that the beam generated in the simulation is within the same general regime as the experimental data obtained from the photocathode rf gun, and there are two particular advantages that the use of a two gas-jet setup would have. It would avoid the problem of synchronizing the beam and the laser, and it would make the use of any rf technology unnecessary, thereby considerably simplifying the experimental setup.

Another important consideration concerns the location and kind of high energy electron generation in the gas jet. Since only the high energy electrons generated over roughly the last 250 $\mu$m are contributing to the final beam, it might be possible to use other gas-jet profiles as long as they maintain the actual rate of decrease in the plasma density over these last 250 $\mu$m. Gas jets, for example, with lower maximum density and a shorter gradient region or higher maximum density and longer gradient should result in the same density slope and therefore in the same beam. The length of the constant density region could be varied as well since it appears to be irrelevant to the electron generation. This means that there should be considerable flexibility in the design of the gas jet used for injection in an experiment.

## IV. DOUBLE-GAS-JET RESULTS

In order to test the concept of using the electron beam generated by the first gas jet for further acceleration in a second gas jet we continued the simulation discussed above. We chose simulations with two different kinds of a second gas jet. Both two-gas-jet simulations assumed a second gas jet of 1500 $\mu$m total width and density gradients of 500 $\mu$m on each side separated from the first gas jet by a distance of $514c/\omega_n$ (66 $\mu$m). The difference between the two cases is the maximum density of the second gas jet. In the first case we used a maximum density of $n_{p2} = 7.07 \times 10^{18}$ $\mathrm{cm}^{-3}$, the same density as in the first gas jet; in the second case we used $n_{p2} = 1.00 \times 10^{18}$ $\mathrm{cm}^{-3}$ as the maximum density.

The importance of this difference in density lies in the fact that the laser will relativistically self-focus at the higher density but not at the lower density [22,23]. For $n_{p2} = 7.07 \times 10^{18}$ cm$^{-3}$ we find for the critical power $P_c = 17(\omega_L/\omega_p)^2 GW = 4$ TW and therefore $P/P_c = 3$. Together with the fact that $L_{\mathrm{FWHM}}/\lambda_p = 1.21$ this means that we can expect to see some relativistic self-focusing which is what we observe in our simulations. The laser pulse there does not diffract over distances longer than a Rayleigh length but largely maintains its shape during the propagation through the plasma. For the case of $n_{p2} = 1.00 \times 10^{18}$ cm$^{-3}$ the corresponding parameters are $P/P_c = 0.42$ and $L_{\mathrm{FWHM}}/\lambda_p = 0.46$. Therefore the laser pulse propagating through this lower density should diffract and lose intensity more quickly which is what we observe in our simulations.

The longitudinal phase space for the two cases at the end of the constant density region is shown in Figs. 5 and 6.

Figure 5 clearly shows that the injection of the electron beam generated in the first gas jet into the second gas jet leads to a strong increase in the energy of the beam but also in an increase in the energy spread. Video 1 shows the evolution of the longitudinal phase space for the whole duration of this simulation. The beam is generated towards the end of the first gas jet and then reaches the second gas jet (starting at frame $12\,768\omega_n^{-1}$, corresponding to 1626 $\mu$m). While the beam moves through the region of increasing density (up to frame $16\,800\omega_n^{-1}$, corresponding to 2139 $\mu$m) no clear increase in the beam energy is recognizable since the beam electrons are experiencing repeatedly accelerating and decelerating fields of the wake generated by the laser. In contrast to this several groups of electrons gain large amounts of energy once the electron beam reaches the area of constant density. Each accelerating phase of the plasma wake accelerates a group of electrons to high energies (up to frame $20\,832\omega_n^{-1}$, corresponding to 2652 $\mu$m). This energy gain is partially lost again when the beam moves through the decreasing density region out of the plasma (up to frame $24\,864\omega_n^{-1}$, corresponding to 3166 $\mu$m). We will discuss the evolution of the beam energy and other beam properties in more detail below.

Figure 6 shows the longitudinal phase space at the same time as Fig. 5, but since the maximum plasma density of the second gas jet in this simulation was only about one-seventh, the result differs in several ways. The increase in the plasma wavelength by roughly a factor of 2.5 leads to fewer plasma wavelengths within the simulation window and to an increase in the number of beam electrons in a given accelerating phase of the plasma wave. The energy gain of the electrons is smaller since the amplitude of the wake is lower and therefore the energy gained over the same distance smaller. Video 2 shows the evolution of the longitudinal phase space over the whole duration of this second simulation. In general the evolution of the beam seen in video 2 is quite similar to the evolution of the beam in video 1 but there are also clear differences due to the different wavelengths and wake amplitudes. In particular, video 2 indicates that the beam does not lose much energy when moving through the density downramp and out of the plasma.

In order to get a better quantitative understanding of these difference we used the data from the simulations to follow the evolution of the different beam properties. The results of this are shown in Figs. 7 and 8.

Figure 7 shows the beam energy, the relative energy spread, the normalized emittance, and the beam charge as functions of the beam propagation through a second

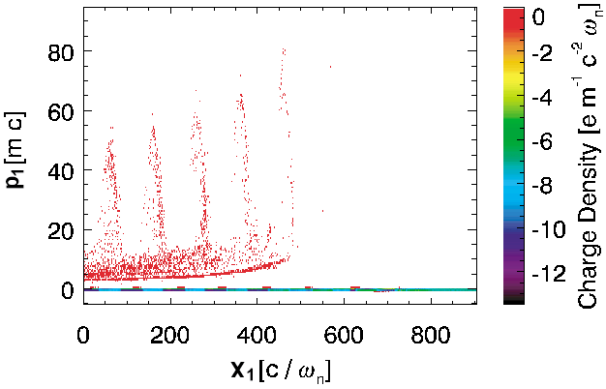


FIG. 5. (Video) The longitudinal phase space density plot at the time when the laser has reached the end of the constant density region of the second gas jet, which has the same density as the first gas jet. The parameters for both gas jets in this simulation are $w_i = 1.5$ mm, $L_{gi} = 0.5$ mm, and $n_{pi} = 7.07 \times 10^{18}$ cm$^{-3}$. The distance between the gas jets is $d = 65$ $\mu$m. See video 1 for the dynamic development of the phase space.

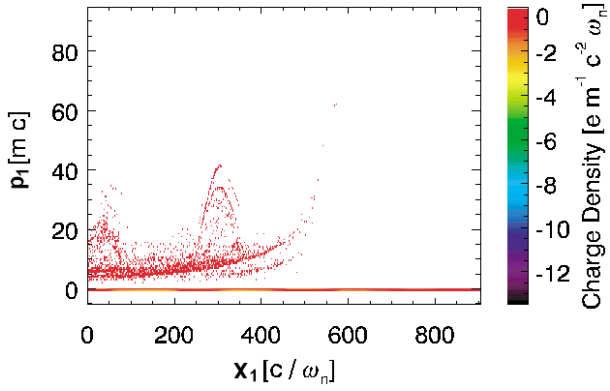


FIG. 6. (Video) The longitudinal phase space density plot at the time when the laser has reached the end of the constant density region of the second gas jet, which has a much lower density than the first gas jet. The parameters for the first gas jet in this simulation are $w_1 = 1.5$ mm, $L_{g1} = 0.5$ mm, and $n_{p1} = 7.07 \times 10^{18}$ cm$^{-3}$. The parameters for the second gas jet are $w_2 = 1.5$ mm, $L_{g2} = 0.5$ mm, and $n_{p2} = 1.0 \times 10^{18}$ cm$^{-3}$. The distance between the gas jets is $d = 65$ $\mu$m. See video 2 for the dynamic development of the phase space.

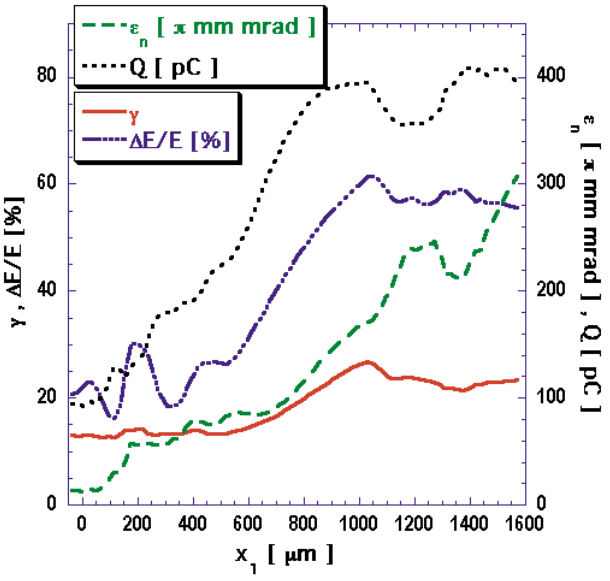


FIG. 7. (Color) The evolution of some important electron beam characteristics from the time after exiting the first gas jet until after exiting the second gas jet. The data are for a second gas jet with $w_2 = 1.5$ mm, $L_{g2} = 0.5$ mm, and $n_{p2} = 7.07 \times 10^{18}$ cm$^{-3}$. The beam energy $\gamma$, the relative energy spread $\Delta E/E$, the normalized emittance $\epsilon_n$, and the beam charge $Q$ are shown. Only electrons with $p_1 \geq 10$ mc were included in the calculation of the numbers shown in the figure.

gas jet with a maximum density of $7.07 \times 10^{18}$ cm$^{-3}$. Note that only electrons with $p_1 \geq 10$ mc were included in the calculations. The evolution of all quantities clearly changes in the three different regions of the gas jet. $\Delta E/E$, $\epsilon_n$, and $Q$ oscillate and increase at the same time while the beam moves through the density upramp. $\gamma$ shows some very small oscillation but is essentially constant during that time. All four quantities increase approximately linearly while the beam is moving through the constant density region. When the beam finally passes through the downramp $Q$ oscillates, $\Delta E/E$ oscillates and decreases slightly, $\gamma$ decreases, and, most importantly, $\epsilon_n$ first makes one oscillation before continuing to increase. The evolution of the beam charge $Q$ is strongly influenced by the fact that only electrons with $p_1 \geq 10$ mc are included in the calculation of the beam quantities. As the beam moves through the second gas jet electrons that were below this threshold at first gain over time enough energy to be included thereby increasing the charge. The additionally included electrons are also contributing to the growth in $\Delta E/E$ and $\epsilon_n$. The most interesting features in Fig. 7 with regard to beam quality are that the beam loses energy and increases in emittance while passing through the density downramp. The final beam characteristics in this simulation after the beam completely passed through the second gas jet are a beam energy $\gamma = 23.5$, an energy spread $\Delta E/E = 56\%$, a normalized emittance $\epsilon_n = 307\pi$ mm mrad, a beam length $l_{\mathrm{FWHM}} = 36.3$ $\mu$m ($121 \times 10^{-15}$ s), and a beam charge $Q = 396 \times 10^{-12}$ C.

Figure 8 shows the beam energy, the relative energy spread, the normalized emittance, and the beam charge as functions of the beam propagation through a second gas jet with a maximum density of $1.00 \times 10^{18}$ cm$^{-3}$. As in Fig. 7 only electrons with $p_1 \geq 10$ mc were included in the calculations. Most features of Fig. 8 are consistent with the remarks made above about Fig. 7. The significant differences, that are caused by the lower density and therefore lower amplitude of the wake, are the following ones. The charge and the emittance of the beam decrease, as the beam moves out of the plasma while the beam energy stays almost constant. This development is consistent with the idea that low energy electrons contribute strongly to the overall emittance of the beam. As the $p_1$ of these low energy electrons drops below 10 mc they do decrease $Q$ and $\epsilon_n$ strongly but do not change $\gamma$ significantly. The final beam characteristics we get after the beam completely passed through the low density gas jet are a beam energy $\gamma = 19.5$, an energy spread $\Delta E/E = 47\%$, a normalized emittance $\epsilon_n = 112\pi$ mm mrad, a beam length $l_{\mathrm{FWHM}} = 38.0$ $\mu$m ($127 \times 10^{-15}$ s), and a beam charge $Q = 277 \times 10^{-12}$ C. The comparison between the results of the two different gas jets clearly indicates that the lower density gas jet has some advantages over the high density gas jet. Even though the beam charge and the energy are slightly lower the emittance has strongly decreased.

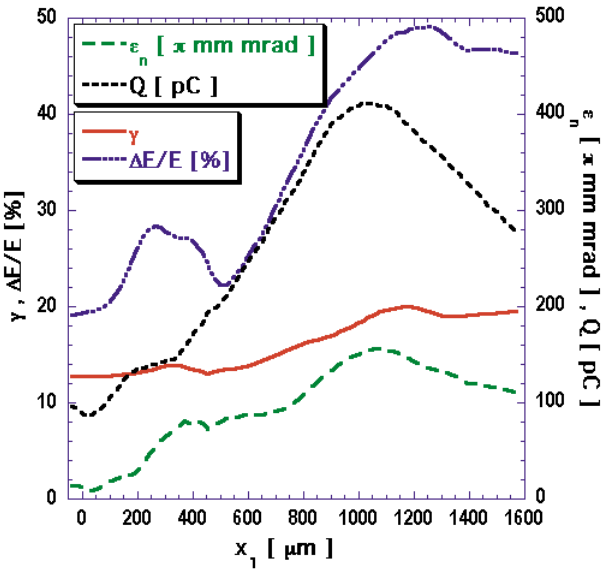


FIG. 8. (Color) The evolution of some important electron beam characteristics from the time after exiting the first gas jet until after exiting the second gas jet. The data are for a second gas jet with $w_2 = 1.5$ mm, $L_{g2} = 0.5$ mm, and $n_{p2} = 1.0 \times 10^{18}$ cm$^{-3}$. The beam energy $\gamma$, the relative energy spread $\Delta E/E$, the normalized emittance $\epsilon_n$, and the beam charge $Q$ are shown. Only electrons with $p_1 \geq 10$ mc were included in the calculation of the numbers shown in the figure.

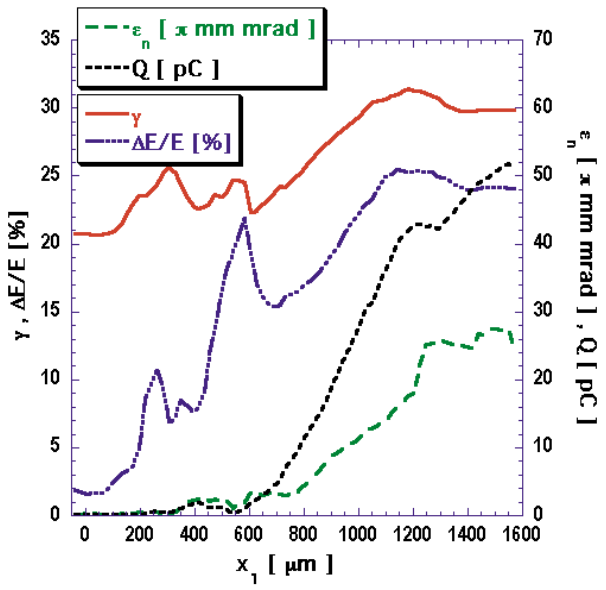


FIG. 9. (Color) The evolution of some important electron beam characteristics from the time after exiting the first gas jet until after exiting the second gas jet. The data are for a second gas jet with $w_2 = 1.5$ mm, $L_{g2} = 0.5$ mm, and $n_{p2} = 1.0 \times 10^{18}$ cm$^{-3}$. The beam energy $\gamma$, the relative energy spread $\Delta E/E$, the normalized emittance $\epsilon_n$, and the beam charge $Q$ are shown. Only electrons with $p_1 \geq 20$ mc were included in the calculation of the numbers shown in the figure.

We note that the beam characteristics can be significantly changed by further raising the cutoff momentum which would correspond in an experiment to selecting particles by energy. Figure 9 shows the data for the same simulations as Fig. 8 but it is including only electrons above $p_1 \geq 20$ mc. At first only very few electrons are above this energy but after the laser and the beam reach the constant density region the charge above 20 mc increases. Remarkably this increase continues even during the propagation through the density downramp. The emittance on the other hand after increasing during the constant density region oscillates when the beam passes the density downramp. The final resulting beam has $\gamma = 29.9$, $\Delta E/E = 24\%$, $\epsilon_n = 25\pi$ mm mrad, $l_{\mathrm{FWHM}} = 37.0$ $\mu$m ($123 \times 10^{-15}$ s), and $Q = 51 \times 10^{-12}$ C.

Using a cutoff momentum of $p_1 \geq 30$ mc changes the beam properties even further. The numbers for this high energy part of the beam are $\gamma = 35.8$, $\Delta E/E = 15\%$, $\epsilon_n = 7\pi$ mm mrad, $l_{\mathrm{FWHM}} = 25.4$ $\mu$m ($85 \times 10^{-15}$ s), and $Q = 12 \times 10^{-12}$ C.

## V. CONCLUSION

Our simulations of a 12 TW LWFA over distances similar to the distances used in experiments showed that a single gas jet can be used to generate a significant number of electrons with generally good beam properties but energies of only about 6 to 7 MeV. We identified the mechanism of the trapping and acceleration of plasma electrons as transverse wave breaking on the density downramp. The crucial parameter that determines the resulting beam seems to be the rate of density decrease over the last approximately 250 $\mu$m of the plasma.

It was possible to accelerate a beam generated in the first gas jet farther by sending the laser pulse and the beam trailing it through a second gas jet. The resulting beam had generally better properties when the second gas-jet densities were low enough to avoid relativistic self-focusing.

Even better results for the beam could probably be obtained if the density gradient width for the second gas jet could be made narrower to minimize the emittance and energy spread growth while passing through the gradients. Another improvement would be to make the second gas jet wider which would lead to larger final energies. At non-self-focusing plasma density longer propagation through the second gas jet would also lead to further diffraction of the laser pulse. This in turn would decrease the magnitude of the accelerating/decelerating and focusing/defocusing forces on the electron beam while it passes through the density downramp. It should finally be noted that these considerations and problems regarding the beam quality are probably relevant for all beams injected in a LWFA, not only to this case where the injected beam was generated in a first gas jet.

## VI. ACKNOWLEDGEMENTS

We would like to thank Warren Mori, Ricardo Fonseca, and James Koga for helpful conversations. This research was made possible by the support from the Japanese Society for the Promotion of Science (JSPS) for one of the authors (R. G. H.).

[1] T. Tajima and J. M. Dawson, Phys. Rev. Lett. **43**, 267 (1979).
[2] P. Sprangle, E. Esarey, A. Ting, and G. Joyce, Appl. Phys. Lett. **53**, 2146 (1988).
[3] E. Esarey, P. Sprangle, J. Krall, and A. Ting, IEEE Trans. Plasma Sci. **24**, 252 (1996), and references therein.
[4] D. Umstadter, Phys. Plasmas **8**, 1774 (2001), and references therein.
[5] N. M. Hafz, Ph.D. thesis, University of Tokyo, 2001.
[6] N. A. M. Hafz *et al.* (to be published).
[7] N. A. M. Hafz *et al.*, in *Proceedings of the 2001 IEEE Particle Accelerator Conference* (IEEE, New York, 2001), p. 3969.
[8] R. G. Hemker *et al.*, in *Proceedings of the 1999 Particle Accelerator Conference*, edited by A. Luccio and W. MacKay (IEEE, New York, 1999), p. 3672.
[9] R. G. Hemker, Ph.D. thesis, University of California, Los Angeles, 2000.
[10] K.-C. Tzeng, W. B. Mori, and C. D. Decker, Phys. Rev. Lett. **76**, 3332 (1996).
[11] D. Umstadter *et al.*, Science **273**, 472 (1996).
[12] C. I. Moore *et al.*, Phys. Rev. Lett. **79**, 3909 (1997).

[13] S.-Y. Chen, M. Krishnan, A. Maksimchuk, and D. Umstadter, Phys. Plasmas **7**, 403 (2000).
[14] A. I. Akhiezer and R. V. Polovin, Sov. Phys. JETP **3**, 696 (1956).
[15] S. V. Bulanov, F. Pegoraro, A. M. Pukhov, and A. S. Sakharov, Phys. Rev. Lett. **78**, 4205 (1997).
[16] S. Bulanov, F. Pegoraro, and J. Sakai, Nucl. Instrum. Methods Phys. Res., Sect. A **410**, 477 (1998).
[17] S. Bulanov, N. Naumova, F. Pegoraro, and J. Sakai, Phys. Rev. E **58**, R5257 (1998).
[18] S. Bulanov *et al.*, Plasma Phys. Rep. **25**, 468 (1999).
[19] H. Suk, N. Barov, J. B. Rosenzweig, and E. Esarey, Phys. Rev. Lett. **86**, 1011 (2001).
[20] M. Reiser, *Theory and Design of Charged Particle Beams* (John Wiley and Sons, New York, 1994).
[21] M. Uesaka *et al.*, IEEE Trans. Plasma Sci. **28**, 1133 (2000).
[22] P. Sprangle, E. Esarey, and A. Ting, Phys. Rev. A **41**, 4463 (1990).
[23] P. Sprangle, E. Esarey, and A. Ting, Phys. Rev. Lett. **64**, 2011 (1990).